

Electron temperatures of a late-phase solar active region from *Yohkoh* BCS and SXT observations

Alphonse C. Sterling^{*,**}

Computational Physics Inc., 2750 Prosperity Ave., Suite 600, Fairfax, VA 22031, USA (asterling@solar.stanford.edu)

Received 19 October 1998 / Accepted 18 February 1999

Abstract. We deduce electron temperatures in a 2–3 month old active region from 1996 September and October, using soft X-ray S XV spectra from the Bragg Crystal Spectrometer (BCS) and images from the Soft X-ray Telescope (SXT), both on board the *Yohkoh* satellite. Our observations cover a full transit of the region, from before its appearance around the east limb until after it disappeared around the west limb. Over most of this transit the region is diffuse and extremely quiescent, with few strong X-ray intensity enhancements (microflares) seen in plots of the *GOES* flux. During the passage the region’s temperature is roughly constant at 2.5 ± 0.2 MK in S XV and at 1.9 ± 0.1 MK from SXT, with emission measures of about 10^{48} cm^{-3} for both instruments. Temperatures obtained from SXT are consistently lower than the S XV values, indicating a multithermal plasma. A high-temperature ($\gtrsim 5$ MK) component, seen in younger active regions, is virtually absent in this mature active region. Our findings, combined with earlier work, provide a method for estimating S XV temperatures of structures based on their intensity in SXT, even when these structures are not isolated on the Sun and hence not directly resolvable with the full-Sun BCS instrument. Our work also suggests that old active regions form a fundamental component of the quiet-Sun corona during periods of high solar activity.

Key words: Sun: atmosphere – Sun: corona – Sun: X-rays, gamma rays

1. Introduction

A perhaps simplistic, but nonetheless common categorization of the solar corona is into active regions, quiet Sun regions, and coronal holes. Active regions seem to have different phases of evolution, with some periods more active than others. We have been making spectral studies of active regions during the recent solar minimum period, using data from the Bragg Crystal Spectrometer (BCS) experiment on board the *Yohkoh* satellite (Ster-

ling 1997a, 1997b; Sterling et al. 1997). Those studies involved relatively young active regions which displayed a large amount of activity. In particular, flares and weaker intensity brightenings, which we call microflares (a.k.a. active region transient brightenings; e.g., Shimizu 1995), were prevalent. Those spectral observations allowed us to determine electron temperatures in active regions both when the regions were on the solar disk, and when they were partially obscured by the solar limb. In this paper, we extend our previous studies by examining the thermal properties of a late-phase active region. In contrast to the earlier studies, this region is very diffuse and quiescent, with no indication of flaring or strong microflaring activity for nearly the entire observation period. (By “strong” microflaring, we mean microflares clearly detectable in the *GOES* soft X-ray channels.) In addition to BCS data, we also deduce temperatures from *Yohkoh*’s soft X-ray telescope (SXT).

Because the *Yohkoh* BCS is a full-Sun instrument, uncontaminated spectra for individual solar features can only be obtained when those features are extremely bright compared to other X-ray solar features. This is generally true for flares, except in uncommon cases when two or more flares occur simultaneously. For active regions, however, the situation is more complicated, since any other active region concurrently on the Sun will also contribute to the BCS spectra. Thus in order to study the properties of a single active region, the observations must occur at times when only a single active region is present on the Sun. *Yohkoh* was launched in 1991 August, when solar activity was high. At such times there was virtually always more than one active region on the solar disk. During the recent solar minimum, however, there have been opportunities to study the spectral properties of isolated active regions, as was done in the studies referred to above.

For the work here, we use data from an active region that developed at the site of a diffuse complex of activity, and became prominent on the Sun around 1996 July 6. It was designated as AR 7978 by the National Oceanic and Atmospheric Administration (NOAA), and made its first crossing of the west solar limb on about July 15. This active region was the most prominent active region on the Sun for several months. It produced a large amount of activity early in its life, including a *GOES*-class X2.6 flare on July 9, many M-flares, and CMEs (e.g., Dryer et al. 1998), with reduced activity after the first

Send offprint requests to: A. Sterling

* Also, E.O. Hulburt Center for Space Research, Naval Research Laboratory, Washington D.C. 20375

** Present address: Institute for Space and Astronautical Science, Yoshinodai 3-1-1, Sagamihara, Kanagawa 229-0022, Japan

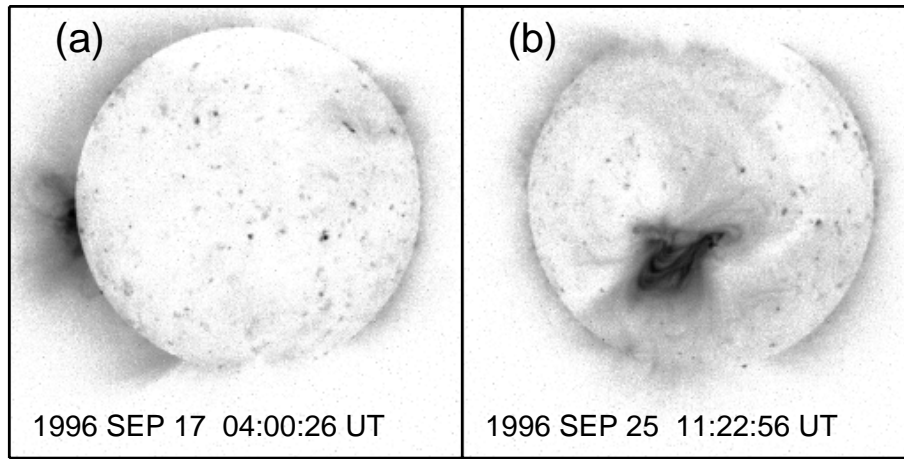


Fig. 1a and b. Images taken with the AlMg filter of SXT **a** when the active region is largely occulted by the east solar limb, and **b** when the region is near disk center. Both images are 5.34 s exposures with SXT's AlMg filter and have $4.91''$ pixel resolution.

disk passage. In subsequent solar rotations, this same activity complex was on the Earthward side of the Sun over the approximate periods July 26–August 9 (when it was re-designated as NOAA 7891), August 22–September 4 (NOAA 7986), September 19–October 2 (too weak for a NOAA designation), and October 17–30 (too weak for a NOAA designation). This is the same region studied by Sterling et al. (1997) as it made its first passage beyond the west solar limb. Hudson et al. (1998) and Harvey & Hudson (1998) discuss other aspects of this same active region.

2. Observations and data analysis

Our observations cover the period 1996 September 10–October 5, which includes the fourth passage of the active region on the disk, including its appearance around the east limb early in that period, and its disappearance around the west limb late in the period. Fig. 1 shows two images from SXT during the period, with west to the right and south downward. Fig. 1a shows the region about two days' rotation behind the east limb and Fig. 1b shows it close to disk-center passage. Both images are 5.34 s exposures with SXT's AlMg filter and have $4.91''$ pixel resolution. Fig. 1b shows that the region is very extended, where the 50%-intensity level covers approximately $600'' \times 450''$. At times during our observation period there also seem to be connections between the brightest parts of the region and surrounding regions, in particular those further to the south.

Yohkoh's BCS (see Culhane et al. 1991 and Lang et al. 1992 for overviews) consists of four channels, covering the resonance lines and principal satellite lines of H-like iron, (Fe XXVI, nominally covering the wavelength range $1.7636\text{--}1.8044 \text{ \AA}$); He-like iron (Fe XXV, $1.8298\text{--}1.8942 \text{ \AA}$), He-like calcium (Ca XIX, $3.1631\text{--}3.1912 \text{ \AA}$), and He-like sulfur (S XV, $5.0160\text{--}5.1143 \text{ \AA}$). Only the S XV channel covers a low enough energy range to observe emissions from non-flaring active regions routinely, and therefore our BCS work here is confined to S XV results.

Even in S XV, the flux from the late-phase active region presented here is so low that we can obtain useful spectra only after extremely long integrations. Also, since the region does not show short time-scale activity (see Fig. 3, introduced below),

there is no need for high time cadence. Accordingly, spectra for the data here are for time intervals ranging from 3120 s to 29 448 s in order to obtain statistically-significant spectra.

As in our previous low-flux spectral studies (e.g., Sterling et al. 1997), we addressed the issue of the background in S XV by obtaining spectra at times when there were no active regions on the Sun. We used data accumulated for some 27 000 s on 1996 September 13 for the background, when the active region was on the far side of the Sun prior to the disk passage of this study. The resulting background spectrum is similar to that found by Sterling et al. (1997) in its magnitude, its variation with time, and its wavelength distribution. For example, a background spectrum integrated for about the same length of time from 1996 October 7, which was a time when the region was behind the Sun after the disk passage of this study, has a magnitude within 15% of that of the September 13 background spectrum over the full wavelength range of the S XV channel. Fig. 2a shows the September 13 background spectrum (multiplied by a “background multiplication factor,” discussed below, of 0.7), as the lower of the two features in the figure. In the same panel, the upper feature is a spectrum integrated for 21 384 s from a time period when the active region is on the disk. Prominent spectral lines are visible in the upper spectrum, and these lines are strikingly absent in the background spectrum. Since the two spectra were accumulated for a comparable amount of time, this clearly indicates that virtually all the emission-line features in the upper spectrum originate from the weak soft X-ray flux of the active region itself.

There is a wavelength dependence of the background spectrum, which shows a broad intensity peak at wavelengths just short of 5.10 \AA . This structured background causes spectra from weak sources to be deformed, and removing some factor times the average background spectrum often improves the shape of the observed spectrum compared to theoretical spectra, as discussed in Sterling et al. (1997). This “background multiplication factor,” however, must be estimated, since we do not have a good understanding of the absolute level of the background at a specified time. For each of the spectra we remove 0.6–1.3 (0.8 on average) times the average background spectrum, where we use the expected near-continuum level fluxes near 5.06 \AA and

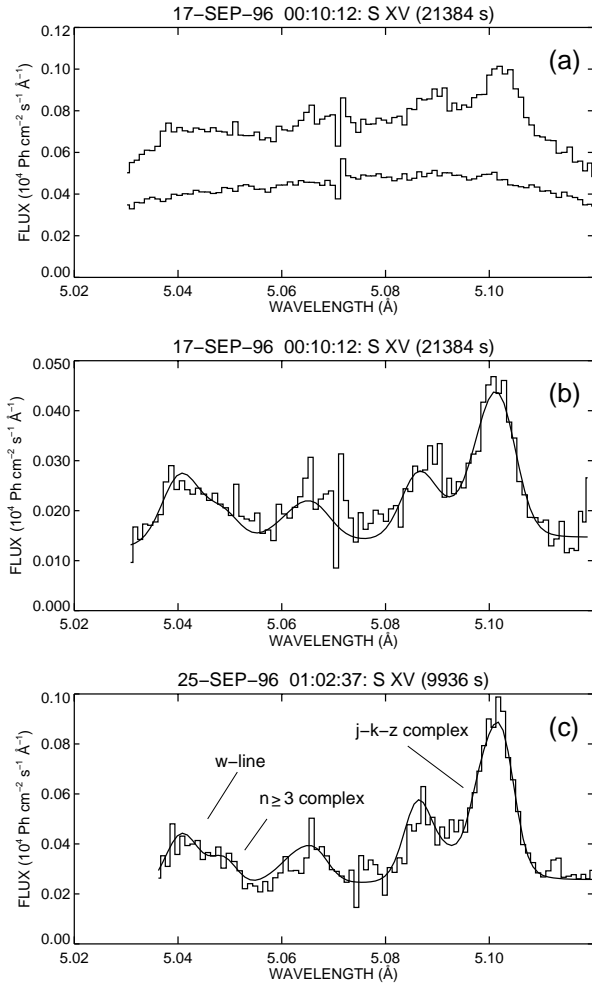


Fig. 2. **a** Spectrum from the late-stage active region from a time when it is only partially occulted (*top histogram*); and an average background spectrum from a time when no active region is on the disk (*bottom histogram*), accumulated for 27 216 s on 1996 September 13 (where the flux level has been multiplied by a “background flux factor” of 0.7). **b** The histogram is the partially occulted spectrum of panel **a** with background spectrum of panel **a** subtracted. The solid line is a best-fitting synthetic spectrum with $T_e = 2.7$ MK. **c** The histogram is a spectrum from the region from a time when it is fully on the solar disk, with the background spectrum shown as the lower plot in panel **a** removed. The solid line is a best-fitting synthetic spectrum with $T_e = 2.41$ MK. The notch near 5.07 \AA is an instrumental artifact.

5.08 \AA to estimate the background multiplication factor. This estimate is made visually, but our resulting resonance line-to-continuum flux ratios are similar to those found during periods of more intense flux and during flares (Fludra et al. 1993), giving us confidence that our resulting background-subtracted continuum levels are reasonable. We will allow for variations in this estimate of the background in our determination of the uncertainties of the electron temperatures from the spectra below.

Fig. 2b shows as a histogram the observed spectrum of Fig. 2a, with the background spectrum of Fig. 2a removed. Overlaid as the solid line is a synthetic S XV spectrum formed using atomic data from Harra-Murnion et al. (1996), and data on

ionization states from Arnaud & Rothenflug (1985). Be-like satellite lines are not included in the fits, but their contribution is not large for the temperatures we deduce from other lines (see Doschek et al. 1996). An isothermal, single temperature component is assumed here and in all our fits (we discuss this assumption in Sect. 3 below), and we obtain the synthetic spectrum that best fits an observed spectrum by seeking the minimum χ^2 value over the approximate wavelength ranges of $5.025\text{--}5.055 \text{ \AA}$ and $5.094\text{--}5.110 \text{ \AA}$. These ranges include lines which are most sensitive to variations in electron temperature, namely, the resonance line (the *w*-line in the notation of Gabriel 1972) near 5.04 \AA , a group of satellite lines including the dielectronic $n \geq 3$ lines near 5.05 \AA , and a blended complex consisting of two dielectronic lines (lines *j* and *k*) and a forbidden line (line *z*) near 5.10 \AA . We assume Voigt profiles for the spectral lines in generating the synthetic spectra. Fits to the observed spectra yield information on the flux, emission measure, electron temperature, and excess line broadenings. In Fig. 2b, the best-fitting spectrum has an electron temperature, T_e , of 2.7 MK. Fig. 2c shows a background-subtracted spectrum from a different time, showing characteristics of slightly cooler plasma at 2.4 MK (the ratio of the *w*-line to the complex at 5.10 is reduced in the lower- T_e spectrum).

We also calculate T_e from SXT using the filter-ratio method (Tsuneta et al. 1991). We used images from the full-frame mode of SXT obtained with the Al.1 and the AlMg filters of exposure times 2.67 and 5.34 s, respectively. We selected several image pairs per day. The cadence of these full-frame images pairs is not great enough to allow us to integrate the SXT images over the approximate time periods of the accumulated BCS spectra. SXT’s partial-frame mode has much higher cadence, but the field of view of the partial frame images is often less than the spatial extent of the active region itself. We therefore opt to use the full-frame images for our analysis, where we can select a sub-image of size large enough to encompass the entire active region. We used sub-images of $810'' \times 810''$, approximately centered on the region, and we integrate the flux over the entire sub-image in calculating the temperatures.

3. Results

Fig. 3a shows soft X-ray fluxes over the times of our study from the $1\text{--}8 \text{ \AA}$ channel of the GOES 9 satellite, with the standard letter designations for the intensity levels given on the right-side axis. The active region was completely behind the Sun until about September 16, and its emergence is marked by an increase in the GOES flux. This shallow increase in flux is in contrast to sharp changes in the flux seen when the region was brighter earlier in its life (e.g., Hudson et al. 1998; Dryer et al. 1998), suggesting a more extended and dimmer emitting volume in its later phases. There is only a slight increase in the GOES level between the times of our background spectrum (which lacks spectral lines) from September 13 data, and the times when the active region is on the disk and emission lines are prominent (see Fig. 2a). By the end of the period, on October 7, the region

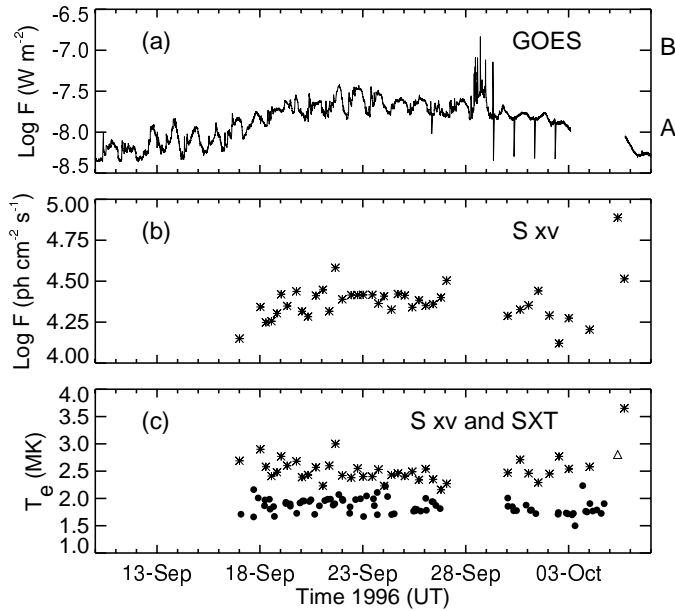


Fig. 3a–c. Time variation of X-ray properties of the late-phase active region. **a** *GOES* (1–8 Å) flux variation with time, with the standard *GOES* alphabetical classification on the right-hand side axis. The diurnal modulation is a satellite artifact. **b** Flux derived from BCS S XV spectra (total flux seen in the channel after removal of an appropriate background spectrum for each datum). **c** Electron temperatures from the S XV spectra (asterisks and triangle), and from SXT (circles). The value represented by the triangle is plotted at 0.5-times its actual value in order to fit on the plot. The S XV and SXT properties are not calculated for a time period around September 28, since at that time there is a flux enhancement from an area of the Sun not associated with the late-phase active region of this study.

has rotated to the far side of the Sun again. There is a gap in the *GOES* data near the time of the disappearance.

A movie constructed from full-frame SXT images shows that there are two brief time periods of substantial flaring activity. The first of these appears as a flux enhancement in the *GOES* data on September 28, and is due to a small spatial scale brightening that occurs in a region separated from the active region of our study. We omit data from this secondary feature in our analysis. The second activity brightening occurs on October 5 (there is a gap in the *GOES* flux at that time in Fig. 3a), when the active region had rotated around the west solar limb, and was associated with the eruption of a large-scale coronal mass ejection (CME) seen in SXT (Watari et al. 1997).

There is a steady oscillation in the *GOES* flux with period of about one day. We believe that this is due to the low solar flux level and the response of the *GOES* sensors to particle background. The peaks correspond to passages of the *GOES* satellite through the anti-solar direction. Since *GOES* is geostationary, it passes through the same magnetospheric tail region roughly once every twenty-four hours, since the belts are approximately stationary with respect to the Sun–Earth axis.

Fig. 3b shows the S XV flux as a function of time. There are no measurable emission line spectra attainable prior to our first datum on September 17. After a rise in intensity between

September 17 and 20 as the region emerges from the East limb, the flux remains very constant. It begins to decrease near the end of the observation period, but there is a strong flux enhancement at the time of the CME-related event on October 5.

Fig. 3c shows T_e values derived from the S XV spectra as asterisks and a triangle. We have determined uncertainties assuming two sources of errors summed in quadrature: the 1σ error associated with the fit to the spectra, and the spread in the resulting temperatures assuming a $\pm 20\%$ change in our primary estimate of the background level (i.e., the background multiplication factor described in Sect. 2). These uncertainties average 0.1 MK, with the largest being 0.3 MK; the uncertainty in the background level contributes most to these values. We do not plot the resulting error bars since they are generally comparable to the size of the asterisks, with the lowest-temperature values generally having the largest errors. The plotted temperatures are the averages of the three values obtained by assuming our primary background level estimate, and the temperatures obtained assuming a $\pm 20\%$ change in the background estimate. One of the temperatures, represented by the triangle, is plotted at 0.5 times its actual value; it is associated with the October 5 CME event and is consequently much higher than the other temperatures. For the 38 data points between September 17 and October 4, the S XV-derived electron temperatures range from 2.26 to 3.03 MK, with an average value and 1σ sample standard deviation of 2.52 ± 0.16 MK.

SXT temperatures are plotted in Fig. 3c as filled circles, and average 1.86 ± 0.14 MK. Statistical uncertainties in the derived SXT temperatures are less than 0.05 MK for all of the points.

SXT and BCS are sensitive to plasmas of differing temperatures, as indicated by their respective signal response functions shown in Fig. 4. The SXT functions are for the two filters used in our analysis, and are derived by convolving the instrument response functions with the theoretical X-ray emission line spectra of Mewe et al. (1985) and the continuum expression of Mewe et al. (1986), as discussed in Tsuneta et al. (1991); these curves use DN s^{-1} units, where $1\text{DN}=100$ electrons created by the CCD (see Hara et al. 1992). For S XV Fig. 4 shows the contribution function given by

$$G(T_e) = F(T_e) \frac{\exp(-\Delta E_{12}/kT_e)}{T_e^{1/2}}, \quad (1)$$

where $F(T_e)$ is the fractional ion abundance in ionization equilibrium, taken from Arnaud & Rothenflug (1985), and ΔE_{12} is the transition energy for the line formation. The two SXT response functions decrease with decreasing temperature below about 5 MK, while that of S XV peaks near 15 MK (e.g., Culhane et al. 1991) and falls more sharply with decreasing temperatures than do the SXT filters. Therefore S XV tends to pick out higher temperatures in the active region than does SXT, and SXT is more sensitive to cooler temperatures than is S XV. So the differing SXT and S XV temperatures can be explained in terms of a multithermal active-region plasma. Fig. 4 also indicates that there is little or no material hotter than the S XV T_e values given in Fig. 3c, since S XV would have a much higher sensitivity to any such hotter material than it does to 2–3 MK material. That

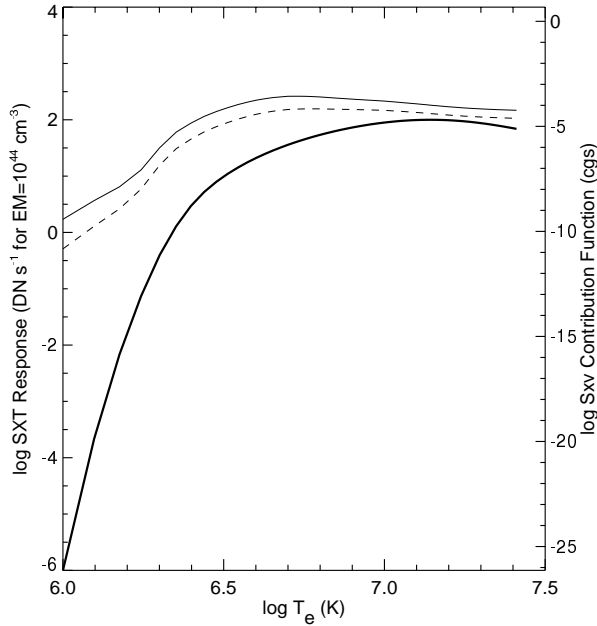


Fig. 4. Plots of the sensitivity functions as functions of temperature for the SXT Al.1 filter (thin solid line), AlMg filter (dashed line) and the contribution function for the BCS Sxv resonance line (thick solid line). The scale for Sxv (right-side) covers many more decades than the scale for the SXT filters (left-side).

is, if a substantial amount of hotter material were present, Sxv would yield T_e values higher than the 2–3 MK we find.

We calculate emission measures,

$$EM = \int n_e^2 dV, \quad (2)$$

where n_e is the electron density and V is the volume of the emitting plasma, using the spectral fit outputs for Sxv and the ratio of the two SXT filter responses for SXT (e.g., Hara et al. 1992). Average log emission measures are 48.3 ± 0.4 for Sxv and 48.1 ± 0.2 for SXT. These values are consistent with studies of active-region loops with SXT. Cargill & Klimchuk (1997), for example, deduce linear emission measures of $0.25\text{--}100 \times 10^{27} \text{ cm}^{-5}$. Those loops had lengths $L \sim 5 \times 10^9 \text{ cm}$, so that an area factor of L^2 imply volume emission measures of $\sim 6 \times 10^{45}\text{--}2.5 \times 10^{48} \text{ cm}^{-3}$. Klimchuk & Gary (1995) also find emission measures of about $10^{28}\text{--}10^{29} \text{ cm}^{-5}$, and Kano & Tsuneta (1995) find similar values. Thus our values for the volume emission measures fall near the upper end of the range of those from those studies, assuming the same area factor as above. Our values are about an order of magnitude higher than some other active region studies, e.g., Pye et al. (1978) found 10^{47} cm^{-3} in the 2–3 MK range using *Skylab* data and Saba & Strong (1991) found about 10^{47} cm^{-3} for an active region at about 3 MK using Mg XI spectra from the FCS instrument on *SMM*. The difference is likely due to the large, diffuse volume of the region we study here.

Because of Sxv’s strong bias toward detecting the highest temperatures in the non-flaring active region, and since the emission measures of the cooler material detectable by SXT are not

much larger than the Sxv emission measures, we expect that the Sxv spectra are not strongly affected by contributions from the cooler material. Thus our single-temperature component assumption used in our fits to the spectra (see Sect. 2) should be a good one.

Non-thermal line broadenings are commonly observed in solar flare spectra (see, e.g., Khan et al. 1995; Mariska et al. 1995; and Harra-Murnion et al. 1997, for discussions of non-thermal broadening in flares obtained from *Yohkoh*’s BCS). There is a difficulty in measuring line widths with BCS for distributed sources, however, as the line widths are affected by the north-south distribution of the emitting source, due to the geometry of the BCS crystals and their mounting orientation on the spacecraft. In the Sxv channel, this broadening due to instrument orientation occurs at the rate of 1.2 km s^{-1} per each $1''$ in the north-south direction (Mariska 1994; Sterling 1997a), where the excess broadening is expressed in terms of an equivalent turbulent velocity. Because of the large extent of the source indicated by the SXT images, we are not able to reliably separate the physical line broadenings from the instrumental line broadenings for this region.

By observing a much more compact region than that of the study here, Sterling (1997a) was able to examine active region non-thermal line broadenings using BCS Sxv data, obtaining an average value of $43.5 \pm 11.8 \text{ km s}^{-1}$. SXT images of that active region at the 50% contour level corresponded to a Sxv line broadening of 15 km s^{-1} , which was small compared to the derived non-thermal velocity values. That region, however, was not as quiescent as the current one is, and so some short-duration, relatively low- or moderate-level (although possibly higher-level than the background *GOES* level in Fig. 3a) microflares may also be included in that analysis.

4. Discussion

Our findings indicate that the X-ray nature of an old, docile active region is considerably different from that of young, “active” active regions. A key differing parameter appears to be the frequency of strong microflares, which are ubiquitous in young active regions, and virtually absent in the region studied here. Some microflares are the source of the hotter temperature component ($T_e \gtrsim 5 \text{ MK}$) in active regions (e.g., Watanabe et al. 1995, Yoshida & Tsuneta 1996, Sterling et al. 1997; see also Feldman et al. 1996), and their paucity in our old active region results in there being no hotter component observed in the Sxv spectra. Our hottest temperatures in this region only reach about 3.0 MK (excluding the brief period of higher activity), and still cooler plasmas exist in the active region also as evidenced by the SXT-derived temperatures of Fig. 3c.

We are not, however, able to say whether *all* microflares are absent in this old active region. Shimizu (1995) and Feldman et al. (1996) indicate that some microflares are extremely weak and have $T_e < 5 \text{ MK}$, and some such low-level microflares may be included over the long integration times we use in our analysis. Nonetheless, Fig. 3a shows that there are very few microflares distinguishable above the *GOES* background level over

the time range of our study here. We can therefore say that the frequency of microflares detectable in *GOES*, i.e. those which were found to be abundant in young, “normal” active regions and often could be linked to the $T_e > 5$ MK hot component, are suppressed in this older active region.

Sterling (1997a) found average S XV T_e values of 5.5–6.2 MK for a younger (and substantially smaller in spatial extent) active region of 1996 March (Porter & Klimchuk, 1995, find similar temperatures for active region coronal loops). That study did not find temperatures as low as those we find here, but there were many microflares occurring throughout the life of that region, and so it is possible that Sterling (1997a) integrated over both hotter and cooler component temperatures when forming spectra in that study. A typical integration time outside times of brighter microflares in that study was 1000–2000 s, and so there may have been several low- to moderate-level shorter-lived microflares occurring during the integrations. It may also be that such microflares occur at such a high frequency in young active regions that their coronal plasmas never have time to cool. Shimizu (1995) gives typical cooling times for microflares to be 40 s due to conduction, and so microflares occurring on this timescale would keep the plasma heated (the radiative cooling time scale is much longer, but the conductive energy loss is two orders of magnitude larger than the radiative loss in his analysis). Since this time scale is shorter than the typical BCS integration times used, we cannot be certain that the 1996 March active region did not have temperatures as low as those we find here.

There is much better agreement between our S XV temperatures here and those of Sterling et al. (1997), who found $T_e \lesssim 2.5$ MK for the isolated upper portions of the same active region studied in this paper when it was very young (about nine days after it became prominent in X-rays). They also found higher temperatures ($T_e \gtrsim 3.0$ MK) at lower altitudes at that time for the region, consistent with the finding that microflares in young active regions are generated at low altitudes (Sterling et al. 1997; Sterling 1997b). The microflares would probably be due to interaction and reconnection between emerging flux and pre-existing coronal fields (e.g., Heyvaerts et al. 1977; Yokoyama & Shibata 1996; Canfield et al. 1996). We believe, therefore, that both Sterling et al. (1997) and our current work see the cool temperature coronal component alone, but for different reasons: Sterling et al. (1997) see it because they are looking high in the active-region corona while the microflares producing the high-temperature component are restricted to heights occulted by the solar limb, and we see only the cool component here because there are no longer enough microflares to produce (or maintain) the hot component.

By using the occultations of active regions by the solar limb, Sterling (1997b) and Sterling et al. (1997) concluded that T_e seen in S XV decreased with height in active regions. We do not see any evidence for a decrease with height in the region studied here. In fact, in contrast to our previous studies, close inspection of Fig. 3c shows a slight downward trend in the S XV T_e values between September 17 and 20, and perhaps a slight increasing trend between October 1 and 4. These time periods respectively correspond to when the active region is emerging from the east

limb and going behind the west limb, and therefore the temperature trends would suggest an *increase* in temperature with height in this region. Such an increase in T_e with height would be expected if, e.g., the region consists of simple, large-scale loops (e.g., Wragg & Priest 1981, Priest et al. 1998), without a hot source (such as microflaring loops) at low altitudes. Moreover, very weak, diffuse regions have been found to show an increase in temperature with height (Sturrock et al. 1997; Wheatland et al. 1997). We do not, however, see a trend with height of the SXT temperatures in Fig. 2c, so the trends seen in S XV could be an aspect of the slightly hotter plasma seen in S XV, the longer averaged integration times of S XV, or they could be a systematic artifact of the BCS analysis. For example, similar to the widths of the spectral lines discussed earlier, the *shape* of the spectra will also depend on the north-south distribution of the intensity of the emitting source, and this distribution will change between when the region is partially occulted and when it is on the disk. This change may alter the spectral shape only modestly, but perhaps enough to generate the weak trends in temperatures we see. We surmise that the trends in temperature and the possible relation to the spectral shape are too subtle for effective analysis, and we are therefore unable to draw strong conclusions about the temperature structure with height in this region. We can only say that any temperature variation with height is weak at best.

As noted in the Introduction, we could not obtain spectroscopic temperatures from BCS for individual solar structures during solar maximum since BCS is a full-Sun instrument. But we can use some of our quiet-Sun results to speculate about the thermal properties of solar features during enhanced-activity periods by comparing intensities of various structures seen in SXT. Fig. 5 shows an AlMg SXT image from near the previous solar activity maximum. Wheatland et al. (1997) analyzed the area labeled as the “Diffuse Region” of this figure. In Fig. 5 that area has an intensity level of $\lesssim 20$ SXT DN s⁻¹. In comparison, our active region in Fig. 1b has an intensity level of 50–250 DN s⁻¹, and the region studied by Sterling (1997a) (Fig. 1 of that paper, also taken with the AlMg filter), has intensity of about 5000–25 000 DN s⁻¹. In Fig. 5, regions labeled “Diffuse Loops” have intensities similar to that of the active region in Fig. 1b, and regions labeled “Bright Loops” have intensities similar to those of the region in Sterling (1997a). Based on this, we speculate that the Bright Loops of Fig. 5 contain both hot and cool temperature coronal plasmas with S XV T_e values around 5.5–6.2 MK (Sterling 1997a), while the Diffuse Loops consist of the cool component only with S XV T_e values similar to those we found in Fig. 3c (~ 2.5 –3 MK). Although we do not directly see in S XV features which have SXT intensities corresponding to the Diffuse Region of Fig. 5, we would guess that they would have S XV temperatures slightly lower than that of the Diffuse Loops, based on an intensity comparison. In this way, using the SXT-intensity S XV-temperature relationship for isolated features on the Sun allows us to estimate the S XV-temperatures for features which cannot be individually resolved by BCS.

This methodology can also be used to address what seems to be a contradiction in some of the previous spectroscopic

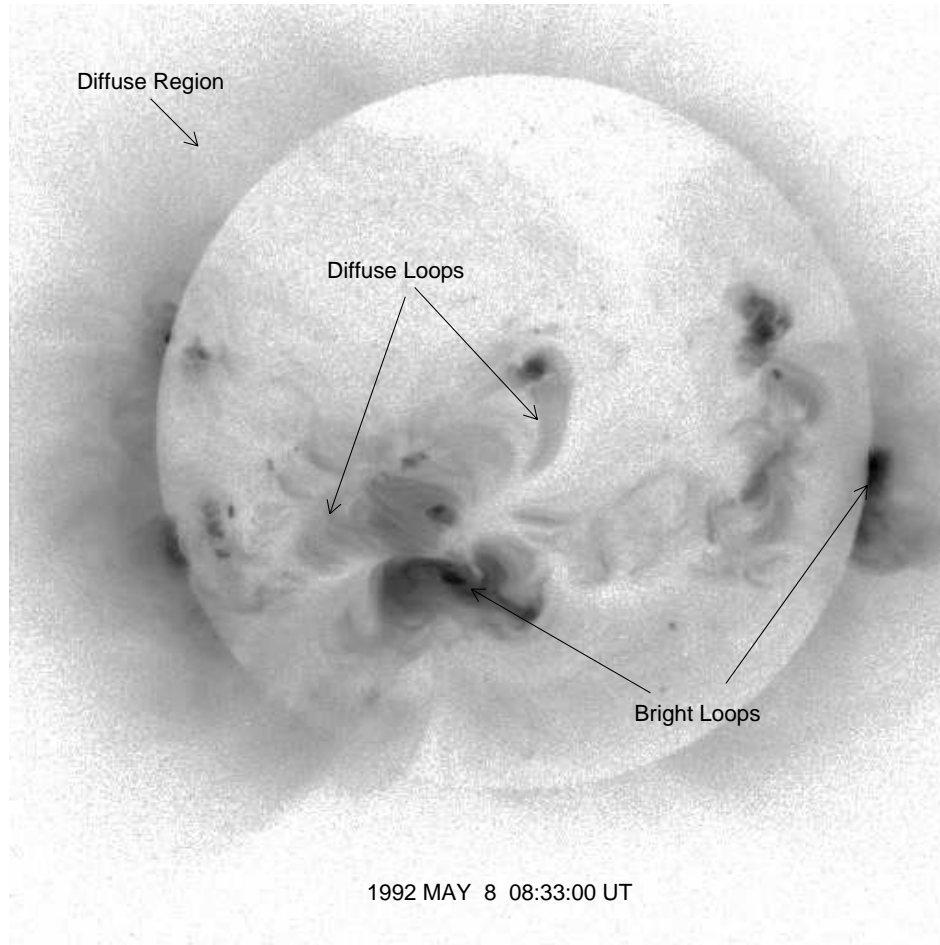


Fig. 5. A 2.67 s exposure SXT AIMg filter image from a time near solar maximum. The region identified as a “Diffuse Region” was studied by Wheatland et al. (1997), and has an intensity level lower than that of the active region of this paper. The “Diffuse Loops” have intensities similar to that of the active region of this paper, and the “Bright Loops” are more intense, with an intensity similar to that of an active region of March 1996 studied by Sterling (1997a).

active region studies. Sterling (1997a) found that S XV electron temperature (average values of 5.5–6.2 MK) from an isolated active region during solar cycle minimum was correlated with the S XV intensity. Similarly, Watanabe et al. (1995) found that the temperature of the corona near solar maximum was higher at a time when the overall coronal flux was higher ($T_e \approx 4$ MK), compared to the temperature at a time two months later ($T_e \approx 2.4$ MK) when the overall coronal flux was lower (but still higher than the coronal flux during solar minimum). The apparent contradiction comes from the fact that the S XV flux of the solar-minimum-period active region studied by Sterling (1997a) was lower than the flux of the corona during the time when Watanabe et al. (1995) measured the $T_e \approx 2.4$ MK temperatures. If the flux-temperature correlation holds generally, we would expect that the temperatures seen by Sterling (1997a) to have been lower than those of Watanabe et al. (1995). Sterling (1997a) speculated that the reason his temperatures were higher than Watanabe et al.’s (1995) may be because, in addition to active regions, there was much more diffuse corona present during the time of the Watanabe et al. (1995) study, and that this diffuse corona may have had a lower temperature than that of Sterling’s (1997a) active region’s corona. When averaged over the entire corona, the overall temperatures would be reduced by the cooler background corona. Our results from the present

study support this picture (we are assuming that the SXT and S XV intensities scale in a similar fashion, which seems reasonable). That is, it is indeed likely that the diffuse background corona in the Watanabe et al. (1995) study had temperatures comparable to those we find in Fig. 3c (and presumably those of the “Diffuse Loops” of Fig. 5 also), bringing down the average temperature of the overall corona in their study.

As *Yohkoh* was launched during the height of solar maximum, it was not possible to see how the diffused regions of the Sun developed. We suspect that much of it comes from old active regions—such as the one studied here—that lose their hotter temperature component, and then become diffuse, e.g., due to the dispersal of the active-region magnetic elements in time as discussed by Leighton (1964). In addition, there may be connections made between these old active regions with different active regions (Tsuneta 1996), thereby forming larger-scale quite Sun coronal features. Another factor possibly contributing to, or augmenting, the magnetic interactions is that the active region studied here was an old solar cycle (cycle 22) region occurring at the start of the new solar cycle (cycle 23), and thus there were magnetic field polarities corresponding to both cycles on the Sun when the region was present (Harvey & Hudson 1998); this factor could distinguish this region from other active regions occurring well within a single cycle. Currently ongoing

Yohkoh SXT observations during the buildup of the new solar cycle hopefully will provide us with an opportunity to see if quiet Sun regions near solar cycle maximum actually do develop from old active regions, as suggested by our work here.

In addition, future analysis of observations from the *SOHO* and *TRACE* satellites will certainly help us in evaluating many of the topics discussed here. Some preliminary progress has already been made. For example, using *SOHO*'s Coronal Diagnostic Spectrometer (CDS) instrument, Fludra et al. (1997) and Matthews & Harra-Murnion (1997) discuss relationships between transition region and coronal structures in the same active region we observe here (but during August 1996, when it is in a more active state than discussed in this paper).

Acknowledgements. I thank L. Culhane, H. Hudson, J. Lemen, T. Watanabe, and J.-P. Wuelser for fruitful discussions, and the referee for useful suggestions. I acknowledge support from the Naval Research Laboratory/Office of Naval Research basic research program. *Yohkoh* is a mission of the Institute of Space and Astronautical Sciences (Japan), with participation from the U.S. and U.K.

References

- Arnaud M., Rothenflug R., 1985, *A&AS* 60, 425
 Canfield R.C., Reardon K.P., Leka K.D., et al., 1996, *ApJ* 464, 1016
 Cargill P.J., Klimchuk J.A., 1997, *ApJ* 478, 799
 Culhane J.L., Hiei E., Doschek G.A., et al., 1991, *Solar Phys.* 136, 89
 Doschek G.A., Feldman U., Dubau J., 1996, *Ultra Low Temperature Sulfur X-Ray Spectra*. In: Bentley R.D., Mariska J.T. (eds.) *Magnetic Reconnection in the Solar Atmosphere*. ASP Conference Series vol. 111, Astronomical Soc. of the Pacific, San Francisco, p. 122
 Dryer M., Andrews M.D., Aurass H., et al., 1998, *Solar Phys.* 181, 159
 Feldman U., Doschek G.A., Behring W.E., 1996, *ApJ* 461, 465
 Fludra A., Culhane J.L., Bentley R.D., et al., 1993, *Adv. Space Res.* 13, No. 9, 395
 Fludra A., Brekke P., Harrison R.A., et al., 1997, *Solar Phys.* 175, 487
 Gabriel A.H., 1972, *MNRAS* 160, 99
 Hara H., Tsuneta S., Lemen J.R., Acton L.W., McTierman J.M., 1992, *PASJ* 44, L135
 Harra-Murnion L.K., Phillips K.J.H., Lemen J.R., et al., 1996, *A&A* 308, 670
 Harra-Murnion L.K., Akita K., Watanabe T., 1997, *ApJ* 479, 464
 Harvey K.L., Hudson H.S., 1998, *The Formation and Evolution of the Coronal Holes Associated with NOAA Region 7978*. In: Watanabe T., Kosugi T., Sterling A.C. (eds.) *Observational Plasma Astrophysics: Five Years of Yohkoh and Beyond*. Kluwer, Dordrecht, p. 315
 Heyvaerts J., Priest E.R., Rust D.M., 1977, *ApJ* 216, 123
 Hudson H.S., Labonte B.J., Sterling A.C., Watanabe T., 1998, *NOAA 7978: The Last Best Old-Cycle Region*. In: Watanabe T., Kosugi T., Sterling A.C. (eds.) *Observational Plasma Astrophysics: Five Years of Yohkoh and Beyond*. Kluwer, Dordrecht, p. 237
 Kano R., Tsuneta S., 1995, *ApJ* 454, 934
 Khan J.I., Harra-Murnion L.K., Hudson H.S., Lemen J.R., Sterling A.C., 1995, *ApJ* 452, L153
 Klimchuk J., Gary D.E., 1995, *ApJ* 448, 925
 Lang J., Bentley R.D., Brown C.M., et al., 1992, *PASJ* 44, L55
 Leighton R.B., 1964, *ApJ* 140, 1547
 Mariska J.T., 1994, *ApJ* 434, 756
 Mariska J.T., Sakao T., Bentley R.D., 1995, *ApJ* 459, 815
 Matthews S.A., Harra-Murnion L.K., 1997, *Solar Phys.* 175, 541
 Mewe R., Gronenschild E.H.B.M., van den Oord G.H.J., 1985, *A&AS* 62, 197
 Mewe R., Lemen J.R., van den Oord G.H.J., 1986, *A&AS* 63, 511
 Porter L.J., Klimchuk J.A., 1995, *ApJ* 454, 499
 Priest E.R., Foley C.R., Heyvaerts, J., et al., 1998, *Nat* 393, 54
 Pye J.P., Evans K.D., Hucheson R.J., et al., 1978, *A&A* 65, 123
 Saba J.L.R., Strong K.T., 1991, *ApJ* 375, 789
 Shimizu T., 1995, *PASJ* 47, 251
 Sterling A.C., 1997a, *ApJ* 478, 807
 Sterling A.C., 1997b, *Geophys. Res. Lett.* 24, No. 18, 2263
 Sterling A.C., Hudson H.S., Watanabe T., 1997, *ApJ* 479, L149
 Sturrock P.A., Wheatland M.S., Acton L.W., 1997, *ApJ* 461, L115
 Tsuneta S., 1996, *ApJ* 456, L63
 Tsuneta S., Acton L., Bruner M., et al., 1991, *Solar Phys.* 136, 37
 Watanabe T., Hara H., Shimizu T., et al., 1995, *Solar Phys.* 157, 185
 Watari S., Watanabe T., Acton L.W., Hudson H.S., 1997, *Limb Events Observed by Yohkoh and Coronal Mass Ejections: A Filamentary Soft X-Ray Structure on 5 October 1996*. In: *Proceedings of the Fifth SOHO Workshop*, Oslo University, Oslo, Norway, ESA SP-404, p. 725
 Wheatland M.S., Sturrock P.A., Acton L.W., 1997, *ApJ* 482, 510
 Wragg M.A., Priest E.R., 1981, *Solar Phys.* 70, 293
 Yokoyama T., Shibata K., 1996, *PASJ* 48, 353
 Yoshida T., Tsuneta S., 1996, *ApJ* 459, 342